The Astrophysical Journal Letters, 935:L35 (8pp), 2022 August 20 https://doi.org/10.3847/2041-8213/ac88c1

The Planetary Nebula in the 500 Myr Old Open Cluster M37

Vasiliki Fragkou[1], Quentin A. Parker[2,3], Albert A. Zijlstra[3,4], Roberto Vázquez[1], Laurence Sabin[1], and Jackeline Suzett Rechy-Garcia[5]
[1] Instituto de Astronomía, Universidad Nacional Autónoma de México, 22800, Ensenada, B.C., Mexico
[2] Department of Physics, The University of Hong Kong, Chong Yuet Ming Physics Building, Pokfulam Road, Hong Kong; quentinp@hku.hk
[3] Laboratory for Space Research, The University of Hong Kong, 405B Cyberport 4, 100 Cyberport Road, Cyberport, Hong Kong
[4] Jodrell Bank Centre for Astrophysics, The University of Manchester, Oxford Road, M13 9PL, Manchester, UK
[5] Instituto de Radioastronomía y Astrofísica, Universidad Nacional Autónoma de México, 58089, Morelia, Michoacan, Mexico
Received 2022 July 27; revised 2022 August 10; accepted 2022 August 10; published 2022 August 23

Abstract

We report confirmation of a large, evolved, bipolar planetary nebula and its blue, white dwarf central star as a member of the ∼500 Myr old Galactic open star cluster M37 (NGC 2099). This is only the third known example of a planetary nebula in a Galactic open cluster and was found via our ongoing program of identifying and studying planetary nebulae—open cluster associations. High confidence in the association comes from the consistent radial velocities and proper motions for the confirmed central star and cluster stars from Gaia, reddening agreement, and location of the planetary nebula well within the tidal cluster boundary. Interestingly, all three Galactic examples have bipolar morphology and likely Type-I chemistry, both characteristics of higher mass progenitors. In this case the progenitor star mass is in the midrange of $\sim 2.8\,M_{\odot}$. It provides a valuable, additional point on the key stellar initial-to-final mass relation independent of cluster white dwarf estimates and also falls in a gap in the poorly sampled mass region. This planetary nebula also appears to have the largest kinematical age ever determined and implies increased visibility lifetimes when they are located in clusters.

Unified Astronomy Thesaurus concepts: Open star clusters (1160); Planetary nebulae (1249)

1. Introduction

Planetary nebulae (PNe) are a brief, typically ∼5000–25,000 yr (Badenes et al. 2015), phase of stellar evolution. The central star of a planetary nebula (CSPN) is the low-mass core of the previous Asymptotic Giant Branch (AGB) star, which has expelled its envelope. The CSPN quickly evolves to become a white dwarf (WD) on the cooling track. If the stellar age is known (i.e., the AGB turn-off age for its initial mass), the object can constrain the initial–final mass relation (IFMR).

Planetary nebulae provide us with vital clues for understanding late-stage stellar evolution and Galactic chemical enrichment. Their strong emission lines allow the determination of abundances, expansion and radial velocities, and CSPN temperatures. PNe yield information on the nuclear burning, dredge up, and mass loss in the stellar progenitor (see Kwitter & Henry 2022 for an excellent recent PN review). PN studies have been hampered by three problems: (i) the previous lack of accurate distances to most Galactic PNe; (ii) obtaining representative PNe samples of the true population diversity (Parker 2022), and (iii) their unknown progenitor masses. The first problem has prospects of resolution via accurate Gaia[6] CSPN distances, though many CSPNe remain too distant and faint for Gaia DR3 and correct CSPN identification remains an issue for some (Parker et al. 2022). The second problem is being addressed by deep, narrow-band, wide-field surveys, e.g., Parker et al. (2005), Drew et al. (2005), and Drew et al. (2014).

For the third problem of progenitor masses, these can only be accurately determined for PNe in Galactic globular and open clusters (OCs). These allow precise distance determinations from color–magnitude diagrams (CMD) and Gaia. Importantly, they provide good progenitor mass estimates from the cluster isochrones and the measured cluster turn-off mass. A proven physical association of an OC with a PN is an extremely valuable probe. It can provide us with: (i) accurate physical characteristics of the PN and its CSPN from the known distance; (ii) the metallicity from the nebula and cluster, and (iii) the age and mass of the progenitor star. We can then study the relation between stellar mass and the PN's chemical enrichment, determined from spectroscopic measurements, and provide additional, independent data for the widely used WD IFMR, e.g., Dobbie et al. (2009), that associates WD properties to their main-sequence progenitors. A well-determined IFMR is crucial for tracing the development of both carbon and nitrogen in entire galaxies but remains currently poorly constrained.

There are currently only four confirmed PNe in Galactic globular clusters (Jacoby et al. 1997) but see Bond et al. (2020) where Gaia proper motions bring doubt to PN JaFu1 being a member of globular cluster Palomar 6. Minniti et al. (2019) proposed four additional PNe candidates identified in several of the ∼50 new globular clusters found in the Galactic bulge from the VVV survey (Saito et al. 2012) but substantial follow-up is needed to confirm any of these.

For OCs on the other hand, before this work, only two PNe had been confirmed as physically associated with Galactic OCs (PN PHR 1315−6555 in the OC Andrews-Lindsay 1, and PN BMP J1613−5406 in the OC NGC 6067), both discovered by

[6] https://www.cosmos.esa.int/web/gaia/dr3

members of our team: Parker et al. (2011) and Fragkou et al. (2019a).[7]

Davis et al. (2019) detected a PN that may be a physical member of an OC in the M31 Local Group galaxy indicating the first discovery of an extragalactic PN-OC pair. They estimate a PN initial mass of $3.38^{+0.03}_{-0.02}$ $M_{\odot}$ and enhanced nitrogen abundance, indicating that hot bottom burning can be evident in relatively low-mass AGB stars. The system's remoteness makes detailed study and robust confirmation requirements, as applied to Galactic counterparts, challenging.

As part of a recent astrophotometric study of M37, Griggio et al. (2022) found that a WD, identified as a high-probability proper motion member of the cluster, is also the likely central star of a previously known PN detected in the IPHAS Hα survey (Drew et al. 2005). This association was first proposed by Frew (2017) and subsequently studied by the first author Fragkou (2019) in the context of a possible association with M37. This was based on nebular emission contamination in the fiber spectra of several M37 cluster stars (Núñez et al. 2017) and the presence of an extended, diffuse emission region near the cluster core in a mosaic of the relevant IPHAS Hα images (see their Figure 4). We prove here the association of the PN with M37 and so add an important object to a very small sample.

2. Association of PN IPHASX J055226.2+323724 with Galactic Open Cluster M37

2.1. The PN

The nebula was discovered and classified as a PN candidate by Sabin (2008) from IPHAS imagery. Here we present new, high-resolution radial velocity data that confirm this rare OC-PN link. The PN is identified as a "true," bipolar, likely Type-I PN in HASH (Parker et al. 2016) as IPHASX J055226.2 +323724 (PNG 177.5+03; HASH ID 31188) where a clearer image than that presented in Núñez et al. (2017) shows its evolved, bipolar nature. It is of very low surface brightness at the ∼5 Rayleigh sensitivity limit of IPHAS (Drew et al. 2005) with a major axis of $445'' \pm 10''$. The PN presents enhancements along the southern edges and a patchy internal structure (see Figure 1). The emission line spectra seen in the cluster stellar fiber spectra for five stars in Figure 5 of Núñez et al. (2017) show high [N II]/Hα ratios, indicative of a likely Type-I (nitrogen enriched) chemistry (Kingsburgh & Barlow 1994).

2.2. The CSPN

Based on Sloan Digital Sky Survey imagery (Gunn et al. 2006) we found the CSPN at R.A.: 05:52:26.18, decl.: 32:37:24.63 (J2000), almost exactly at the PN's geometric center (<10″ displacement) which is ∼7.′2 across its major axis. This is also the only blue star within a 116″ radius from the PN's center, making it the only plausible CSPN candidate (see Figure 2). This CSPN was previously identified as a WD candidate in Gentile Fusillo et al. (2015). It is also reported as a CSPN by Chornay & Walton (2020) via Gaia searches for CSPN based on PN in the HASH catalog (Parker et al. 2016), though no association with the cluster was made.

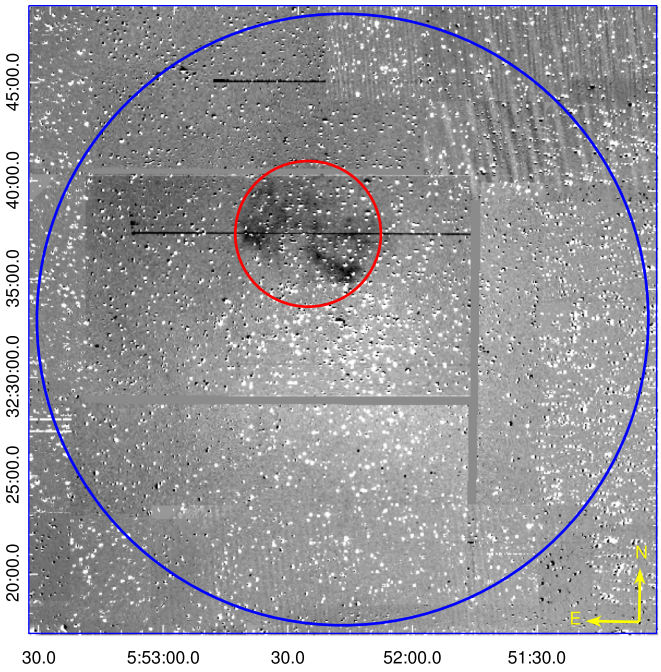

Figure 1. A contrast-enhanced $30' \times 30'$ quotient (H$\alpha - r$ band) IPHAS (Drew et al. 2005) mosaic centered on the core of Galactic open cluster M 37 (NGC 2099). The low surface brightness bipolar PN (IPHASX J055226.2 +323724) is encompassed by a red circle with a diameter of $445'' \pm 10''$ (the nebular major axis) while the blue circle indicates the full ∼30′ extent of the cluster. The PN is well within the cluster tidal radius with the blue CSPN at almost the precise geometric center of the PN. The CSPN is itself only ∼280″ from the published cluster center position.

Low dispersion spectroscopy of the CSPN is presented in Griggio et al. (2022) that show both He II and C IV absorption lines, confirming the CSPN is a hot, hydrogen deficient WD. It is reported as an intermediate type between the DO class and the PG1159 stars, e.g., Werner & Herwig (2006) and Reindl et al. (2014). They report a stellar $T_{\rm eff} > 60{,}000$ K. (We estimate a value closer to 100,000 K in this paper). Hence, this CSPN is hot enough to ionize the observed PN. The Gaia EDR3 ID of this CSPN is 3451205783698632704.

The white dwarf has been classified as a rotating variable with a period of 0.445 days and amplitude of 0.074 mags by Chang et al. (2015; V1975 in their sample). Rotational variability has previously been found in hot DQ white dwarfs (Lawrie et al. 2013; Williams et al. 2016) where it is related to strong magnetic fields. The current star is not known to be of DQ type but this raises the possibility that it could be a transition object between PG1159 stars and DQ white dwarfs. Alternatively, the variability could be due to a close binary; however, it is not classified as such by Chang et al. (2015).

2.3. The Cluster M37 (NGC 2099)

M37 (NGC 2099) is the brightest and richest Galactic open cluster in the constellation of Auriga with a stellar mass of $\sim 1500\,M_{\odot}$ based on concordant Gaia EDR3 (Gaia Collaboration et al. 2021) high-probability proper motions and potentially with as many as 4500 stars. It is a well-studied, intermediate-age (∼500 million-year-old) cluster first discovered by the Italian astronomer Giovanni Battista Hodierna before 1654 and cataloged by Messier in 1781. It is about 30′

[7] BMP J1613−5406's association with NGC 6067 is based on radial velocity, reddening and distance agreement, location of the PN within the cluster's tidal radius, and other considerations. The GAIA DR3 proper motion is inconclusive on this source, with the proper motion differing from that of the cluster by 2.3σ; however, the slightly higher RUWE (renormalized error) of 1.3 indicates an enhanced uncertainty, and the star is very close to the Gaia magnitude limits.

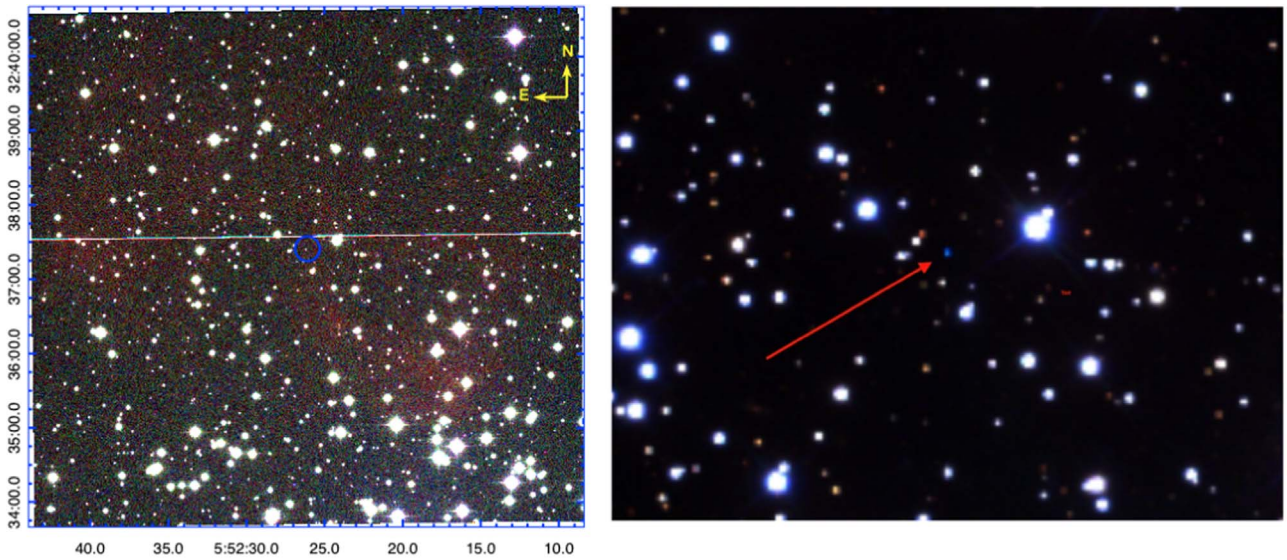

Figure 2. Figure 2(a) left panel: An enhanced $6\farcm5 \times 6\farcm5$ color-composite RGB image of PN IPHASX J055226.2+323724 from the IPHAS survey (Drew et al. 2005) that we confirm as a physical member of the Galactic open cluster M37. Red = Hα, Green = broad band red, and Blue = broad band "*i*". The CSPN is circled in blue; Figure 2(b) right panel: $190 \times 145''$ RGB image created from SDSS with red = *i*, green = *r* and blue = *g*-band. These data clearly show the faint CSPN (arrowed) at the center. North is top, and east is to the left in both images.

across at full extent. Previous modern work includes Kalirai et al. (2001, 2005) and Ahumada & Lapasset (2007) who show the cluster contains three blue stragglers while its hottest surviving main-sequence star is a B9V. More recent work on M 37 concentrates on the Gaia data, e.g., Griggio & Bedin (2022) and Griggio et al. (2022) who also list seven cluster WD candidates, including the CSPN labeled WD 1 in their list. The weighted average cluster physical parameters obtained from the literature have been previously estimated as: angular diameter = $31\farcm15$, age = 470 ± 50 Myr, reddening $E(B-V) = 0.26 \pm 0.04$, distance = 1.44 ± 0.13 kpc and metallicity [Fe/H] = 0.03 ± 0.28 (Griggio & Bedin 2022; refer Table 6.6 in Fragkou 2019). Using 1136 stars with a cluster membership probability >0.8, Cantat-Gaudin et al. (2018) yield a Gaia DR3 mean distance of 1485 pc with $\sigma = 110$ pc, in good agreement with previous estimates. Since this is based on the latest Gaia DR3 data, we are using this cluster distance value throughout. The same stars present a Gaia mean pmRA = 1.88 ± 0.18 mas yr^{-1} and pmDec = -5.62 ± 0.16 mas yr^{-1}. The Gaia DR3 CSPN proper motion is in tight agreement with the cluster average, strongly supporting cluster membership (Table 1). The parallax has a larger uncertainty but is consistent within 1σ. For the adopted cluster distance and angular diameter, the cluster's physical radius is 6.73 pc.

3. Methods

3.1. Magnitudes of the CSPN

The ugriz CSPN magnitudes have been measured from SDSS DR10 (An et al. 2007) as $u = 18.702 \pm 0.020$ mag, $g = 8.978 \pm 0.010$ mag, $r = 19.300 \pm 0.011$ mag, $i = 20.248 \pm 0.063$ mag and $z = 19.840 \pm 0.082$ mag (Gentile Fusillo et al. 2015). Following Jester et al. (2005) these are transformed to the Johnson–Cousins system as $B = 19.07 \pm 0.02$ and $V = 19.16 \pm 0.02$. The errors have been computed with standard error propagation with the transformation rms residuals added quadratically. The CSPN is also included in the Pan-STARRS catalog (Chambers et al. 2016) with magnitudes $g = 19.06 \pm 0.015$, $r = 19.40 \pm 0.01$, $i = 19.69 \pm 0.02$, $z = 19.93 \pm 0.03$, and $v = 20.03 \pm 0.04$.

3.2. Spectroscopic Observations of the PN

For PN radial velocity measurement, we obtained observations with the high spectral resolution MEGARA spectrograph (García-Vargas et al. 2020) on 2022 January 12 (with full moon contamination) and 2022 March 4 (dark sky). MEGARA is an optical (3650-9750 Å) medium-high spectral resolution fiber-fed spectroscopic instrument on the 10.4 m Gran Telescopio CANARIAS (GTC) in La Palma, Canary Islands. We obtained optical spectroscopy at seven distinct positions across the PN (refer to Figure 3(a)). Multiple 5 minutes exposures were taken in IFU mode. The IFU is a bundle of 567 ($0\farcs62$ diameter) fibers that subtend $12\farcs5 \times 11\farcs3$ on the sky. One pointing was centered on the CSPN (pointing a), plus an offset sky exposure. The VPH grating setup was the "HR–R" highest dispersion mode ($R = 20{,}000$) that covers 6400–6800 Å and gives a radial velocity precision of around 1 km s^{-1}, ideal for our purpose. Four areas (a, b, c and d) of the total of the seven pointings were observed in both 2022 January and March. The earlier data was affected by the Moon causing a strong Hα absorption feature but the [N II] and [S II] lines were unaffected. The pointing map and an example combined nebula spectrum from pointings a, b, c, d (for observations made on 2022 March 4) are shown in Figures 3(a), (b).

3.3. Radial Velocity, Kinematic Age, and Electron Density Estimates of the PN

The robust MEGARA pipeline was employed to reduce the data in a standard fashion for IFU mode. Flux calibration and accurate sky subtraction are not essential for the current purposes. The wavelength calibration appears robust. The radial velocities for each pointing are measured from the nebular emission lines in the integrated IFU spectrum of each pointing. After the standard reduction with the MEGARA pipeline (which also combined the exposures for each observing block), the integrated 1D spectrum

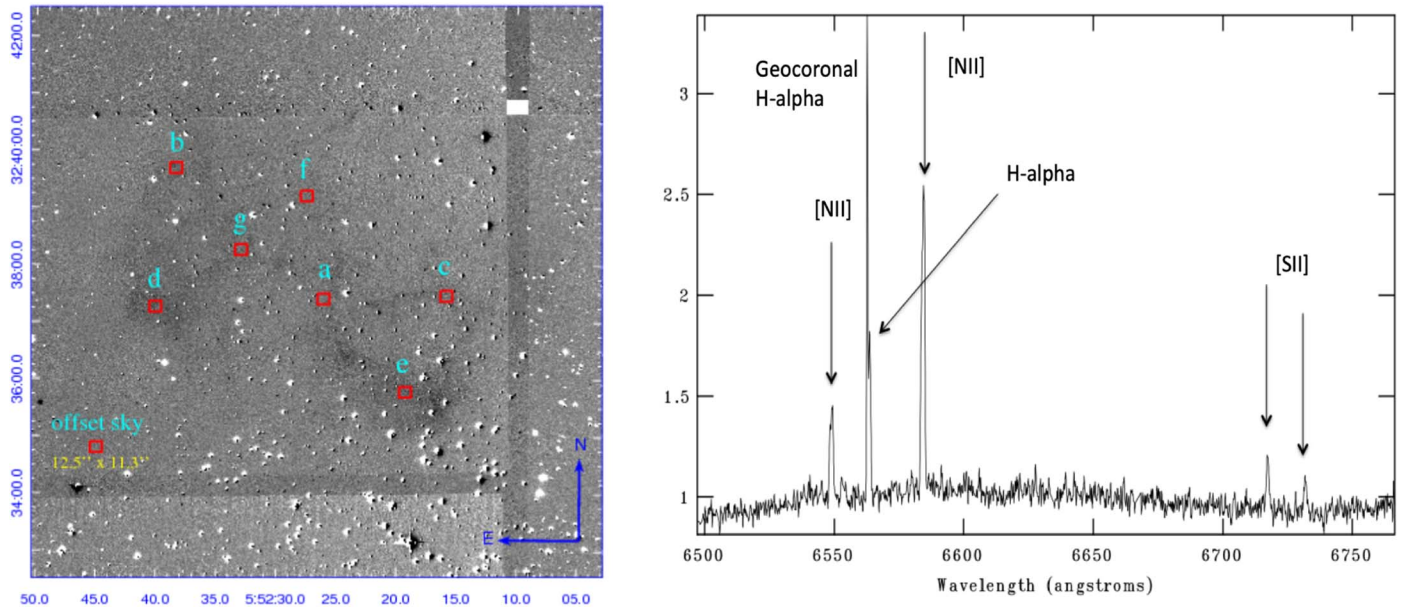

Figure 3. Left panel: PN image with MEGARA IFU pointings indicated. Right panel: a combined 1D continuum subtracted example PN spectrum from 2022 March 4 for IFU pointings a, b, c, and d. The five visible PN emission lines are labeled.

Table 1
Determined PN, CSPN, and Cluster Parameters from This Work and the Literature

Parameter	PN/CSPN	Cluster M37
R.A. (J2000)	05:52:26.191	05:52:18.00
decl. (J2000)	32:37:24.89	32:33:12.00
Apparent diameter (arcmin)	7.42	31.15
Radial Velocity	10.61[a], $\sigma = 4.93$ km s^{-1}	8.32 ± 0.56 km s^{-1}
Distance	same as cluster[b]	1.49 ± 0.11 kpc
Expansion velocity	20,[c] $\sigma = 6.2$ km s^{-1}	
Reddening $E(B-V)$	0.24 ± 0.03[d]	0.26 ± 0.04
Electron density N_e	5 cm^{-3} [e]	
Physical radius	1.60 pc	6.73 pc
Morphology	Bipolar	open cluster
Chemistry	likely Type I	$(Fe/H) = 0.03 \pm 0.28$
Age	$78 \times 10^3 \pm 25 \times 10^3$ yr	470 ± 50 Myr
Estimated nebular mass	0.32 $M_\odot$	
Estimated CSPN $T_{\rm eff}$	100 ± 20 kK	
Estimated CSPN Luminosity $\log L/L_\odot$	1.49 ± 0.25	
Proper motion pmRA (mas yr^{-1})[f]	2.00 ± 0.39	1.88 with $\sigma = 0.18$
Proper motion pmDec (mas yr^{-1})	-5.37 ± 0.22	-5.62 with $\sigma = 0.16$
Central star V magnitude	19.16 ± 0.02	
Central star absolute magnitude M_V	7.56 ± 0.19[g]	
Central star initial mass	$2.78^{+0.12}_{-0.1}$ $M_\odot$	
Central star final mass	$0.63^{+0.03}_{-0.04}$ $M_\odot$	
Central star of PHR 1315-6555 initial mass[h]	2.25 ± 0.13 $M_\odot$	
Central star of PHR 1315-6555 final mass	$0.58^{+0.14}_{-0.08}$ $M_\odot$	
Central star of BMP J1613-5406 initial mass	$5.58^{+0.62}_{-0.43}$ $M_\odot$	
Central star of BMP J1613-5406 final mass	0.94 ± 0.11 $M_\odot$	

Notes.
[a] median of all nebular MEGARA exposures.
[b] We assume the identified blue star is the CSPN.
[c] calculated from the split of the [N II] 6584 line.
[d] as estimated from the CSPN colors.
[e] as implied by the median of the [S II] 6716/6731 line ratios of the four nebular MEGARA exposures acquired on 2022 March 4.
[f] PN proper motions refer to Gaia DR3 data for the identified CS, while cluster proper motions refer to Gaia DR3 median of cluster members with membership probability >0.8 from Cantat-Gaudin et al. (2018).
[g] as derived for the adopted cluster distance and reddening.
[h] initial and final mass values for the other two OC-PN are taken from Fragkou et al. (2019b).

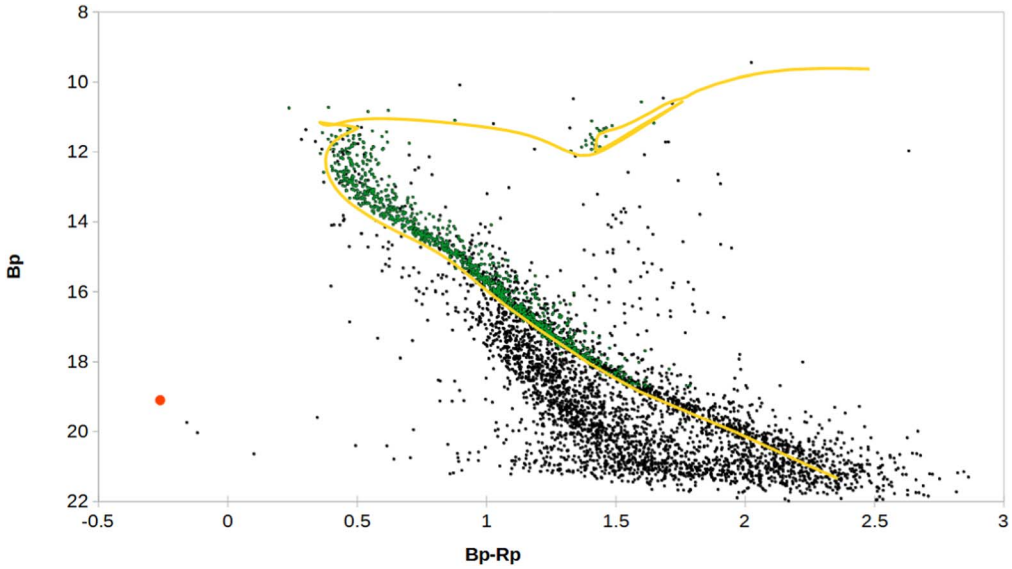

Figure 4. Cluster Gaia DR3 CMD (B vs. B-R) diagram fitted with a Padova theoretical isochrone (Bressan et al. 2012; Marigo et al. 2013) for adopted cluster parameters (age = 470 ± 50 Myr, reddening $E(B-V) = 0.26 \pm 0.04$, distance = 1.49 ± 0.13 kpc and metallicity [Fe/H] = 0.03 ± 0.28). The CSPN is indicated by the red filled symbol. Stars with >80% probability (Cantat-Gaudin et al. 2018) of being a cluster member, based on Gaia DR3 data, are plotted as green dots. The CMD includes all stars with pmRA = 0–4 and pmDec = −8 to −2 mas yr^{-1} (most probable cluster members based on mean proper motions) within 15′ from the cluster's apparent center.

for each pointing was constructed using standard IRAF techniques. The S/N for one of our pointings (area f) from 2022 January 13 was too low for useful measurements. Otherwise the nebular emission lines were used for radial velocity determinations via Gaussian fitting.

We computed the radial velocity average for all pointings with repeated observations (more than one observing block) and calculated the median heliocentric corrected radial velocity of all pointings as $v_{\rm rad} = 10.6 \pm 4.9$ km s^{-1} from six individual combined IFU pointings (four were observed twice on different nights). The nebular spectra covered the [N II], Hα, and [S II] emission lines which were all detected. The weaker [N II] 6548 Å and [S II] doublet lines had too low S/N in individual pointings to give reliable radial velocities due to larger errors. The 6584 Å [N II] line (from all individual observing blocks) and the Hα line (from observations acquired in March and not affected by the strong Hα absorption feature) have both been employed for the calculation of the mean nebular radial velocity. This value is compatible with the cluster heliocentric corrected velocity of $v_{\rm rad} = 8.32 \pm 0.56$ km s^{-1} providing a tight constraint for cluster membership. In most pointings the [N II] 6584 Å line was split into a blueshifted and redshifted component, with various asymmetries. allowing a direct measurement of the nebula expansion velocity at those pointings. The pointing "a" on the PN center provided the clearest splitting of the [N II] 6584 Å line. These provided an average expansion velocity of 20 km s^{-1} with a standard deviation of 6.2 km s^{-1}. This is typical for a PN and allows a kinematic age to be determined from the PN physical size from its angular extent and distance, of $t_{\rm kin} \sim 78 \times 10^3 \pm 25 \times 10^3$ yr. This kinematic age is at the extreme end for PNe as befits such an evolved, large and low surface brightness example. It may in fact be the largest PN kinematic age ever determined, assuming invariant expansion velocity over time.

For the [S II] line electron density estimate, we combined the a, b, c, d pointings from 2022 March 4 to provide a higher S/N, 1D PN continuum subtracted spectrum. A box-3 smooth was applied before Gaussian fits to the two well detected [S II] lines using a wide wavelength range around the lines for determining the best base level. As expected the [S II] lines are found to be in the low-density limit with [S II]6717/6731 ∼ 1.45 ± 0.20 from repeat measures. As such, an electron density of $N_e <$ 5 cm^{-3} was obtained using the IRAF *nebular* add-on package and assuming a $T_e = 10{,}000$ K. We use this value, the average of the nebular minor and major physical radius, and an assumed filling factor of 0.3 (Pottasch 1996) to calculate a maximum ionized PN gas mass of 0.32 $M_\odot$ (Boffi & Stanghellini 1994). From the same data, we measured a [N II]/Hα = 3.58 ± 0.10, which supports the Type I nature of the bipolar nebula.

3.4. Interstellar Extinction

O5 main-sequence stars present a $B-V$ color of −0.33 (Cox 2000), and since hotter stars are expected to have almost identical colors, we use this to estimate the CSPN reddening $E(B-V) = (B-V) - (B-V)_0$. Hence, the $B-V = -0.092$ CSPN color implies a reddening of $E(B-V) = 0.24 \pm 0.03$, in excellent agreement with the cluster weighted average from the available literature of $E(B-V) = 0.26 \pm 0.04$. The Gaia magnitudes are reported in Griggio et al. (2022). An interstellar extinction profile was derived from the 3D galactic model of Vergely et al. (2022) retrieved through EXPLORE.[8] It is an approximately linear rising trend until about 500 pc, has a shallower slope then to 1000 pc with A_o of ∼0.5 and flattens thereafter, rising only to A_o of ∼0.57 by 2000 pc. The main interstellar clouds are at 200 pc, 400 pc, and 1 kpc, with another cloud at 1.6 kpc just behind M37. There is no extinction associated with the cluster itself. This also supports the interpretation of the nebula as a PN rather than ionized interstellar material.

4. M37 Cluster CMD, CSPN Properties, and the Initial-to-final Mass Relation

An M37 cluster CMD (B versus $B-R$) diagram is shown in Figure 4, as generated from Gaia DR3 data and fit with an appropriate Padova theoretical isochrone for the adopted cluster

[8] https://explore-platform.eu

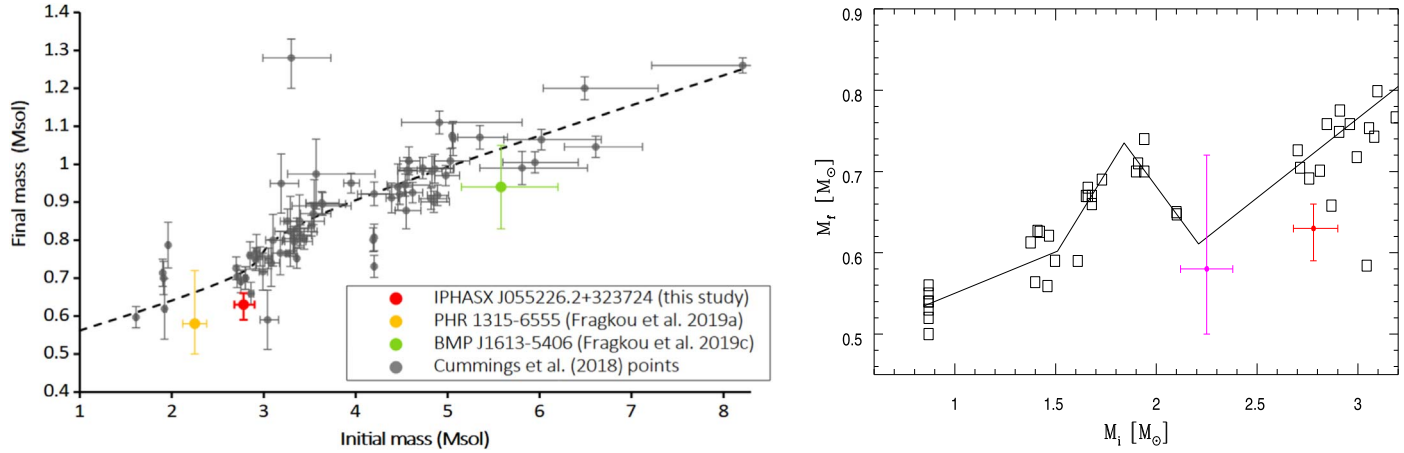

Figure 5. Left panel: a plot from the known sample of cluster white dwarfs for the latest IFMR estimates and semiempirical "PARSEC" fit (Cummings et al. 2018) together with our estimated point for PN IPHAS J055226.2+323724 plotted as a red circle. The other two points from known open-cluster PNe are plotted as a yellow circle (PHR 1315-6555 Fragkou et al. 2019b and Parker et al. 2011) and a green circle (BMP J1613-5406 - Fragkou et al. 2019a). The errors attached to our point reflect the errors in the adopted cluster parameters and the spread of the estimated central star magnitudes. Right panel: the initial–final mass relation of Marigo et al. (2020) with the two cluster PNe within this mass range

parameters (age $= 470 \pm 50$ Myr, reddening $E(B-V) = 0.26 \pm 0.04$, distance $= 1.49 \pm 0.13$ kpc and metallicity [Fe/H] $= 0.03 \pm 0.28$) as the yellow track; see Bressan et al. (2012) and Marigo et al. (2013). The CSPN is shown by a red filled symbol and falls where WD cluster members are expected. Stars with >80% probability (Cantat-Gaudin et al. 2018) of being a cluster member are plotted as green dots. The CMD includes all stars with pmRA $= 0$–4 and pmDec $= -8$ to -2 mas yr^{-1} (most probable cluster members based on mean proper motions) within 15′ from the cluster's apparent center.

4.1. CSPN Derived Parameters

From the adopted cluster parameters and considering the time for the star to leave the main sequence and pass through the RGB/AGB phase, the adopted isochrone predicts a PN progenitor mass of $2.78^{+0.12}_{-0.1}$ $M_\odot$.

For the adopted CSPN V magnitude, cluster reddening, and distance, the CSPN absolute V magnitude is $M_V = 7.56 \pm 0.19$. By plotting the CSPN V magnitude and nebular kinematic age along with evolutionary tracks (see, e.g., Weston et al. 2009, their Figure 1, but using the Miller Bertolami 2016 improved tracks), we estimate a CSPN final mass of $0.63^{+0.03}_{-0.04}$ $M_\odot$ which is well within the expected range for a WD descended from a progenitor star of $\sim 2.8\, M_\odot$.

The CSPN absolute V magnitude and a series of possible CSPN effective temperature values (50–300 kK, in steps of 10 kK) were used to calculate a series of CSPN luminosities, which were plotted along with the corresponding evolutionary track (Miller Bertolami 2016). From the intersection of our line with the evolutionary tracks we estimate a CSPN effective temperature of 100 ± 20 kK (assuming a 20% error). This leads to a CSPN luminosity estimate of $\log L/L_\odot = 1.49 \pm 0.25$.

4.2. The IFMR

The known sample of cluster WDs for the latest IFMR estimates and semiempirical PARSEC fit (Cummings et al. 2018) is presented in Figure 5. Our new estimate for the initial and final mass for our M37 cluster PN IPHAS J055226.2+323724 is plotted as a red circle. The other two colored points are for the other known Galactic OC PNe; PHR 1315-6555 Parker et al. (2011) and Fragkou et al. (2019b) plotted as a yellow circle and the very high mass progenitor of PN BMP J1613-5406, Fragkou et al. (2019a) plotted as a green circle. The errors on each point reflect errors in the adopted cluster parameters and the spread of the estimated CSPN magnitudes.

The OC PNe fall below the plotted dashed line trend from the cluster WDs, which barely overlap with the error bars. Recently Marigo et al. (2020) found an increase in final masses for initial masses in the range 1.5–2 $M_\odot$, based on white dwarfs in the clusters R 137 and NGC 7789. Beyond this excursion the final masses fall back to the previous relation. The putative "kink" is proposed to be related to carbon star formation on the Asymptotic Giant Branch. The interpretation is complicated by having only a single WD star in the range 2–2.5 $M_\odot$ from cluster NGC 752. The location of the two lower initial mass OC CSPN, the cluster white dwarfs, and the proposed relation of Marigo et al. (2020) from their Figure 1 are shown in our version as Figure 5(b). Their errors in M_f are $\sim 0.5\, M_\odot$ but only $\sim 0.05\, M_\odot$ in M_i. Both cluster CSPN trace the key mass range just above the kink and in fact accentuate it, with one in the middle of the empty mass range 2–2.7 $M_\odot$. These cluster CSPN are consistent with the proposed reduction in this mass range from Marigo et al. (2020).

5. Discussion and Conclusions

Confirming an association of a PN and a star cluster requires close agreement of multiple parameters for the PN, CSPN, and cluster. These include PN positional proximity within the cluster tidal radius, reddening and distance agreement, a plausible CSPN, consistent PN and CSPN parameters, and crucially, radial velocity concurrence and proper motion agreement. OC velocity dispersions are typically ~ 1 km s^{-1} so agreement here is a particularly tight constraint. The CSPN of IPHASX J055226.2+32372 passes all these tests and crucially, the radial velocity is in excellent agreement within the errors. There is therefore high confidence that the CSPN and its PN reside in the M37 cluster, one of only three known physical associations of a PN with an OC in our Galaxy.

All results for the PN IPHASX J055226.2+32372, CSPN, and M37 cluster estimated here and those summarized from the

available literature are provided conveniently in Table 1. All key conditions necessary to associate the PN and CSPN with the cluster are shown to be well satisfied. The kinematic age of 78 Kyr appears to be the largest ever determined, assuming the measured expansion velocity has remained invariant with time.

The three Galactic OC PNe come from relatively high (and in one case, very high) progenitor masses. They have notable commonalities. All are bipolar and appear to have Type-I chemistry and high [N II]/Hα ratios. In the two cases of higher progenitor mass, the PNe are highly evolved and physically very large. As higher mass stars evolve quickly through the PN phase to enter the white dwarf cooling track this naturally leads to faint central stars and fainter nebulae. These open clusters have now revealed such nebulae, which are very rare among the known field PNe.

The large PN age found raises the issue of the maximum observable lifetime of PNe in general (Wareing et al. 2007). Any PN shell is limited by interaction with the interstellar medium (ISM). By the time the shell has swept up more mass than its own ejecta, momentum conservation will cause it to adopt the ISM velocity while the CSPN moves with its own peculiar velocity and can leave the PN behind. The nebula eventually loses its structure and dissipates into the ambient ISM. The three Galactic OC-PN uncovered so far all appear to avoid this fate. Stars in OCs have very little velocity dispersion with a systemic velocity likely very close to that of the ISM itself. This limits PN disruption so it is conceivable that OC PNe can be seen for longer than those in the field. In the case of the M37 PN, the brightening of the shell toward the south may herald the interaction with the ISM that will eventually disrupt it.

OC PNe give important IFMR constraints. All three known Galactic examples fall just below the established relation (Cummings et al. 2018). One traces the WD high mass end and one falls in the gap around 2–2.5 $M_{\odot}$. The PNe show that the proposed steepening of the increase of WD masses seen at $M_i \sim 1.6\,M_{\odot}$ to 1.9 (Marigo et al. 2020) does not continue toward higher masses but drops back to the previous level, consistent with that paper's model.

V.F. is in receipt of a UNAM postdoctoral fellowship. This work was supported by UNAM-PAPIIT grant IN106720. Q.A. P. thanks the Hong Kong Research Grants Council for GRF research support under grants 17326116 and 17300417. LS acknowledges UNAM-PAPIIT grant IN110122. This publication is based on data obtained with the MEGARA instrument at the GTC, installed in the Spanish Observatorio del Roque de los Muchachos, in the island of La Palma under program GTC1/21BMEX. MEGARA has been built by a Consortium led by the Universidad Complutense de Madrid (Spain) and the Instituto de Astrofsica, Optica y Electronica (Mexico), Instituto de Astrofsica de Andaluca (CSIC, Spain), and the Universidad Politecnica de Madrid (Spain). MEGARA is funded by the Consortium institutions, GRANTECAN S.A. and European Regional Development Funds (ERDF), through Programa Operativo Canarias FEDER 2014–2020. This work made use of the University of Hong Kong/Australian Astronomical Observatory/Strasbourg Observatory Hα Planetary Nebula (HASH PN) database, hosted by the Laboratory for Space Research at the University of Hong Kong; the extinction map query page, hosted by the Centre for Astrophysics and Planetary Science at the University of Kent; and of data products from the IPHAS survey. This research has made use of the SIMBAD database and the VizieR catalog access tool, CDS, Strasbourg, France (doi:10.26093/cds/vizier). The original description of the VizieR service was published in Ochsenbein, Bauer & Marcout (2000). This work has made use of data from the European Space Agency (ESA) mission Gaia (https://www.cosmos.esa.int/gaia), processed by the Gaia Data Processing and Analysis Consortium (DPAC, https://www.cosmos.esa.int/web/gaia/dpac/consortium). This research has used data, tools, or materials developed as part of the EXPLORE project that has received funding from the European Unions Horizon 2020 research and innovation program under grant agreement No. 101004214. We gratefully acknowledge the earlier work of our colleague Dr. David Frew who first brought this important candidate to our attention in 2017. We thank our colleague Dr. Ivan Bojicic for his help with the creation of the cluster mosaic. We are grateful for the efficient work of the anonymous referee who has helped us improve the paper.

Facilities: GTC:10.4 m, MEGARA; INT 2.5 m & IPHAS.

Software: IRAF (Tody 1986, 1993), MEGARA pipeline (Pascual et al. 2022).

ORCID iDs

Vasiliki Fragkou https://orcid.org/0000-0002-8634-4204
Quentin A. Parker https://orcid.org/0000-0002-2062-0173
Albert A. Zijlstra https://orcid.org/0000-0002-3171-5469
Roberto Vázquez https://orcid.org/0000-0002-3279-9764
Laurence Sabin https://orcid.org/0000-0003-0242-0044
Jackeline Suzett Rechy-Garcia https://orcid.org/0000-0002-0121-2537

References

Ahumada, J. A., & Lapasset, E. 2007, A&A, 463, 789
An, D., Terndrup, D. M., & Pinsonneault, M. H. 2007, ApJ, 671, 1640
Badenes, C., Maoz, D., & Ciardullo, R. 2015, ApJL, 804, L25
Boffi, F. R., & Stanghellini, L. 1994, A&A, 284, 248
Bond, H. E., Bellini, A., & Sahu, K. C. 2020, AJ, 159, 276
Bressan, A., Marigo, P., Girardi, L., et al. 2012, MNRAS, 427, 127
Cantat-Gaudin, T., Jordi, C., Vallenari, A., et al. 2018, A&A, 618, A93
Chambers, K. C., Magnier, E. A., Metcalfe, N., et al. 2016, arXiv:1612.05560
Chang, S. W., Byun, Y. I., & Hartman, J. D. 2015, AJ, 150, 27
Chornay, N., & Walton, N. A. 2020, A&A, 638, A103
Cox, A. N. 2000, Allen's Astrophysical Quantities (New York: AIP Press)
Cummings, J. D., Kalirai, J. S., Tremblay, P. E., Ramirez-Ruiz, E., & Choi, J. 2018, ApJ, 866, 21
Davis, B. D., Bond, H. E., Ciardullo, R., & Jacoby, G. H. 2019, ApJ, 884, 115
Dobbie, P. D., Napiwotzki, R., Burleigh, M. R., et al. 2009, MNRAS, 395, 2248
Drew, J. E., Gonzalez-Solares, E., Greimel, R., et al. 2014, MNRAS, 440, 2036
Drew, J. E., Greimel, R., Irwin, M. J., et al. 2005, MNRAS, 362, 753
Fragkou, V. 2019, PhD thesis, Univ. of Hong Kong
Fragkou, V., Parker, Q. A., Zijlstra, A. A., Crause, L., & Barker, H. 2019a, NatAs, 3, 851
Fragkou, V., Parker, Q. A., Zijlstra, A., Shaw, R., & Lykou, F. 2019b, MNRAS, 484, 3078
Frew, D. J. 2017, in IAU Symp. 323, Planetary Nebulae: Multi-Wavelength Probes of Stellar and Galactic Evolution, ed. X. Liu, L. Stanghellini, & A. Karakas (Cambridge: Cambridge Univ. Press), 11
Gaia Collaboration, Brown, A. G. A., Vallenari, A., et al. 2021, A&A, 649, A1
García-Vargas, M. L., Carrasco, E., Mollá, M., et al. 2020, MNRAS, 493, 871
Gentile Fusillo, N. P., Gänsicke, B. T., & Greiss, S. 2015, MNRAS, 448, 2260
Griggio, M., & Bedin, L. R. 2022, MNRAS, 511, 4702
Griggio, M., Bedin, L. R., Raddi, R., et al. 2022, MNRAS, 515, 1841
Gunn, J. E., Siegmund, W. A., Mannery, E. J., et al. 2006, AJ, 131, 2332
Jacoby, G. H., Morse, J. A., Fullton, L. K., Kwitter, K. B., & Henry, R. B. C. 1997, AJ, 114, 2611

Jester, S., Schneider, D. P., Richards, G. T., et al. 2005, AJ, 130, 873
Kalirai, J. S., Richer, H. B., Reitzel, D., et al. 2005, ApJL, 618, L123
Kalirai, J. S., Ventura, P., Richer, H. B., et al. 2001, AJ, 122, 3239
Kingsburgh, R. L., & Barlow, M. J. 1994, MNRAS, 271, 257
Kwitter, K. B., & Henry, R. B. C. 2022, PASP, 134, 022001
Lawrie, K. A., Burleigh, M. R., Dufour, P., & Hodgkin, S. T. 2013, MNRAS, 433, 1599
Marigo, P., Bressan, A., Nanni, A., Girardi, L., & Pumo, M. L. 2013, MNRAS, 434, 488
Marigo, P., Cummings, J. D., Curtis, J. L., et al. 2020, NatAs, 4, 1102
Miller Bertolami, M. M. 2016, A&A, 588, A25
Minniti, D., Dias, B., Gómez, M., Palma, T., & Pullen, J. B. 2019, ApJL, 884, L15
Núñez, A., Agüeros, M. A., Covey, K. R., & López-Morales, M. 2017, ApJ, 834, 176
Parker, Q. A. 2022, FrASS, 9, 895287
Parker, Q. A., Bojičić, I. S., & Frew, D. J. 2016, JPhCS, 728, 032008
Parker, Q. A., Frew, D. J., Miszalski, B., et al. 2011, MNRAS, 413, 1835
Parker, Q. A., Phillipps, S., Pierce, M. J., et al. 2005, MNRAS, 362, 689
Parker, Q. A., Xiang, Z., & Ritter, A. 2022, Galax, 10, 32
Pascual, S., Cardiel, N., & Gil De Paz, A. 2022, guaix-ucm/megaradrp: Release v0.12.1, Pica4x6, Zenodo, doi:10.5281/zenodo.593647
Pottasch, S. R. 1996, A&A, 307, 561
Reindl, N., Rauch, T., Werner, K., et al. 2014, A&A, 572, A117
Sabin, L. 2008, PhD thesis, Univ. of Manchester, School of Physics and Astronomy
Saito, R. K., Hempel, M., Minniti, D., et al. 2012, A&A, 537, A107
Tody, D. 1986, Proc. SPIE, 627, 733
Tody, D. 1993, in ASP Conf. Ser. 52, Astronomical Data Analysis Software and Systems II, ed. R. J. Hanisch, R. J. V. Brissenden, & J. Barnes (San Francisco, CA: ASP), 173
Vergely, J. L., Lallement, R., & Cox, N. L. J. 2022, arXiv:2205.09087
Wareing, C. J., Zijlstra, A. A., & O'Brien, T. J. 2007, MNRAS, 382, 1233
Werner, K., & Herwig, F. 2006, PASP, 118, 183
Weston, S., Napiwotzki, R., & Sale, S. 2009, JPhCS, 172, 012033
Williams, K. A., Montgomery, M. H., Winget, D. E., Falcon, R. E., & Bierwagen, M. 2016, ApJ, 817, 27